C Journal of Carbon Research

MDPI

Communication

H_2 Adsorption on Small Pd-Ni Clusters Deposited on N-Doped Graphene: A Theoretical Study

Brenda García-Hilerio, Lidia Santiago-Silva, Adriana Vásquez-García, Alejandro Gomez-Sanchez, Víctor A. Franco-Luján and Heriberto Cruz-Martínez *

Tecnológico Nacional de México/IT del Valle de Etla, Abasolo S/N, Barrio del Agua Buena, Santiago Suchilquitongo 68230, Oaxaca, Mexico; brenda.hilerio@itvalletla.edu.mx (B.G.-H.); lidiasilva0008@gmail.com (L.S.-S.); adriana.vasquez@itvalletla.edu.mx (A.V.-G.); alejandro.gs@itvalletla.edu.mx (A.G.-S.); victor.fl@itvalletla.edu.mx (V.A.F.-L.)
* Correspondence: heriberto.cm@itvalletla.edu.mx

Abstract: The study of novel materials for H_2 storage is essential to consolidate the hydrogen as a clean energy source. In this sense, the H_2 adsorption on $Pd_{4-n}Ni_n$ (n = 0–3) clusters embedded on pyridinic-type N-doped graphene (PNG) was investigated using density functional theory calculations. First, the properties of $Pd_{4-n}Ni_n$ (n = 0–3) clusters embedded on PNG were analyzed in detail. Then, the H_2 adsorption on these composites was computed. The E_{int} between the $Pd_{4-n}Ni_n$ (n = 0–3) clusters and the PNG was greater than that computed in the literature for Pd-based systems embedded on pristine graphene. Consequently, it was deduced that PNG can more significantly stabilize the $Pd_{4-n}Ni_n$ (n = 0–3) clusters. The analyzed composites exhibited a HOMO–LUMO gap less than 1 eV, indicating good reactivity. Based on the E_{ads} of H_2 on $Pd_{4-n}Ni_n$ (n = 0–3) clusters embedded on PNG, it was observed that the analyzed systems meet the standards set by the DOE. Therefore, these composites can be viable alternatives for hydrogen storage.

Keywords: Bimetal clusters; ADFT calculations; H_2 storage; 2D materials

Citation: García-Hilerio, B.; Santiago-Silva, L.; Vásquez-García, A.; Gomez-Sanchez, A.; Franco-Luján, V.A.; Cruz-Martínez, H. H_2 Adsorption on Small Pd-Ni Clusters Deposited on N-Doped Graphene: A Theoretical Study. *C* **2024**, *10*, 73. https://doi.org/10.3390/c10030073

Academic Editor: Jorge Bedia

Received: 15 July 2024
Revised: 8 August 2024
Accepted: 10 August 2024
Published: 13 August 2024

1. Introduction

Hydrogen has garnered substantial attention for use as a clean energy source because it possesses a higher energy content per unit weight [1–4]. A critical challenge associated with hydrogen is the low density under standard conditions. Consequently, different hydrogen storage technologies have been proposed to improve the storage density [5,6]. The liquefaction, compression, or a combination of these two methods are commonly used strategies for hydrogen storage [7,8]. Nevertheless, these technologies are not economically feasible [7,8]. Therefore, the research on hydrogen storage in materials has increased considerably in the past few years [7], considering that novel materials with hydrogen storage properties have sufficiently catered to the standards specified by the U.S. Department of Energy (DOE) [9,10].

Nowadays, numerous researchers have analyzed the feasibility of various materials for use in hydrogen storage [11,12]. The graphene-based structures have gained significant attention due to favorable properties such as good conductivity, high thermal/chemical stability, and high specific surface area [13,14]. Although graphene-based structures may be viable alternatives for hydrogen storage, pristine graphene structures exhibit limited chemical reactivity for hydrogen storage [15]. Consequently, different strategies have been used to improve chemical reactivity of graphene, highlighting the use of defects. It has been reported that defective graphene structures exhibit better reactivity properties compared to pristine graphene [15–18]. Among the different types of defects implemented in graphene, the use of pyridinic N_3-doped graphene (PNG) has been highlighted [19–21].

In some studies, PNG properties have been improved by supporting metal atoms or clusters on its surface, which helped to derive optimal properties for different appli-

cations [22–24]. At a theoretical level, different metal clusters embedded on PNG have been investigated for hydrogen storage [25–29]. For instance, density functional theory (DFT) calculations were used to study the hydrogen adsorption on Pd_n clusters (n = 1–4) embedded on PNG structures [25,26]. In another study, the first-principle computations were employed to study the hydrogen storage on a Sc atom embedded on PNG [27]. More recently, Rh_2 and Ti_2 dimers embedded on PNG were studied for hydrogen sorption using DFT computations [28]. Finally, the DFT-based computations were employed to investigate the hydrogen storage on a Cu atom embedded on PNG [29]. Among the systems studied, the Pd clusters embedded on PNG structure can be highlighted, since they present promising results for hydrogen storage [25,26]. However, Pd is an expensive and scarce metal. Therefore, Pd alloyed with 3*d* metals is a well-established strategy to reduce the Pd content in various other applications [30,31]. Also, it is necessary to explore the use of Pd-based bimetal clusters embedded on PNG as materials for hydrogen storage, considering that bimetal clusters exhibit significantly different properties with respect to monometal clusters. In this sense, in this study, the H_2 adsorptions on small $Pd_{4-n}Ni_n$ (n = 0–3) clusters embedded on PNG were studied using DFT calculations. First, the properties of $Pd_{4-n}Ni_n$ (n = 0–3) clusters embedded on PNG were explored. Then, the H_2 adsorption sites and energies on $Pd_{4-n}Ni_n$ (n = 0–3) clusters embedded on PNG were computed.

2. Computational Details

All computations were carried out using the auxiliary DFT (ADFT) implemented in the deMon2k program [32]. For the exchange and correlation contributions, the revised PBE functional was employed [33]. The variational fitting approach was employed to calculate the Coulomb energy [34]. The 18-electron QECP | SD basis set was used for the Pd atoms [35], and the remaining atoms were described using the DZVP-GGA basis set [36]. All computations were performed considering the GEN-A2* auxiliary function set [36]. The restricted open-shell Kohn–Sham computations were performed to avoid spin contaminations for open-shell systems [37]. All structures were optimized in the delocalized internal coordinates that employed the quasi-Newton method [38]. The computational methodology used in this investigation has been previously validated [21,39] and the results obtained agreed with the experimental evidence.

First, the most stable structures for the $Pd_{4-n}Ni_n$ (n = 0–3) clusters were obtained from the literature [40,41] and reoptimized in this study. To analyze the properties of $Pd_{4-n}Ni_n$ (n = 0–3) clusters embedded on PNG, the PNG structure used in this study is illustrated in Figure 1. We selected this structure because it has been widely utilized to represent the graphene structure [42–44]. To obtain the most stable interaction between the Pd_4 cluster and the PNG, four different interactions were proposed and optimized, while, for the bimetal $Pd_{4-n}Ni_n$ (n = 1–3) clusters and the PNG, ten different structures were considered and optimized for each system. The interaction energies (E_{Int}) between the $Pd_{4-n}Ni_n$ (n = 0–3) clusters and the PNG were calculated by employing an equation reported in the literature [21]. For a detailed understanding of the interaction between the $Pd_{4-n}Ni_n$ (n = 0–3) clusters and the PNG, bond critical points (BCPs) and the Bader charge between the $Pd_{4-n}Ni_n$ (n = 0–3) clusters and the PNG were calculated. Finally, to gain insights into the reactivity of the studied systems, frontier molecular orbitals were calculated.

Finally, to obtain the most stable H_2 adsorption on $Pd_{4-n}Ni_n$ (n = 0–3) clusters embedded on PNG, various initial adsorptions were investigated. The H_2 adsorption energies (E_{ads}) on $Pd_{4-n}Ni_n$ (n = 0–3) clusters embedded on PNG were calculated using the following equation:

$$E_{ads} = E_{H2/cluster/PNG} - (E_{H2} + E_{cluster/PNG})$$

where $E_{H2/cluster/PNG}$ is the energy of the H_2 molecule adsorbed on $Pd_{4-n}Ni_n$ (n = 0–3) clusters embedded on PNG and where E_{H2} and $E_{cluster/PNG}$ are the total energy computed for H_2 molecules and $Pd_{4-n}Ni_n$ (n = 0–3) clusters embedded on PNG, respectively.

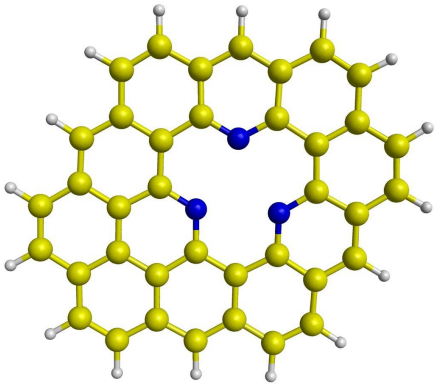

Figure 1. The PNG structure. Blue, yellow, and white spheres represent N, C, and H atoms, respectively.

3. Results and Discussion

3.1. Properties of $Pd_{4-n}Ni_n$ (n = 0–3) Clusters Embedded on PNG

The most stable interactions between the $Pd_{4-n}Ni_n$ (n = 0–3) clusters and the PNG are reported in Figure 2. For the Pd_4 structure embedded on PNG, it was observed that the interaction occurs with a Pd atom in the PNG vacancy, which agrees with the most stable interaction reported in the literature for this system [25,45]. For the Pd_3Ni_1 structure embedded on PNG, it was observed that the interaction occurred through the Ni atom in the PNG vacancy. For the $Pd_{4-n}Ni_n$ (n = 2 and 3) clusters embedded on PNG, the interactions were through two Ni atoms (one Ni atom in the PNG vacancy and the other Ni atom attached to the carbon atoms of the PNG). On the spin multiplicity of $Pd_{4-n}Ni_n$ (n = 0–3) clusters embedded on PNG, all composites presented a spin multiplicity of 4 (quartet) (Table 1). As the systems studied are open-shell, it is important to know their spin density distributions. The computed results for the $Pd_{4-n}Ni_n$ (n = 0–3) clusters embedded on PNG are illustrated in Figure 3. It was observed that the spin density was located mainly on the metal atoms.

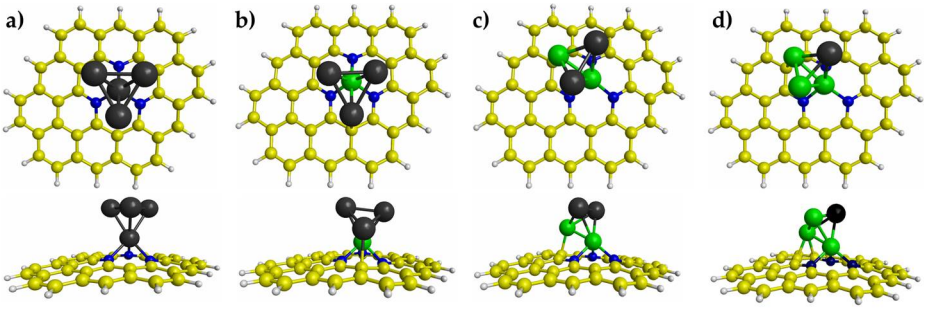

Figure 2. The most stable interactions between the $Pd_{4-n}Ni_n$ (n = 0–3) clusters and the PNG. (**a**) Pd_4 cluster embedded on PNG, (**b**) Pd_3Ni_1 cluster embedded on PNG, (**c**) Pd_2Ni_2 cluster embedded on PNG, and (**d**) Pd_1Ni_3 cluster embedded on PNG. Blue, yellow, white, green, and black spheres represent N, C, H, Ni, and Pd atoms, respectively.

Table 1. Spin multiplicities, Bond critical points (BCPs), interaction energies (E_{int}), Bader charge analysis, and the HOMO–LUMO gap of the $Pd_{4-n}Ni_n$ (n = 0–3) clusters embedded on pyridinic N-doped graphene (PNG).

	Pd_4/PNG	**Pd_3Ni_1/PNG**	**Pd_2Ni_2/PNG**	**Pd_1Ni_3/PNG**
Spin multiplicities	4	4	4	4
BCPs	3	3	4	5
E_{int} (eV)	−2.74	−4.37	−5.00	−5.50
Bader charges (e)	0.39	0.54	0.65	0.74
HOMO–LUMO gap (eV)	1.0	0.91	0.71	0.69

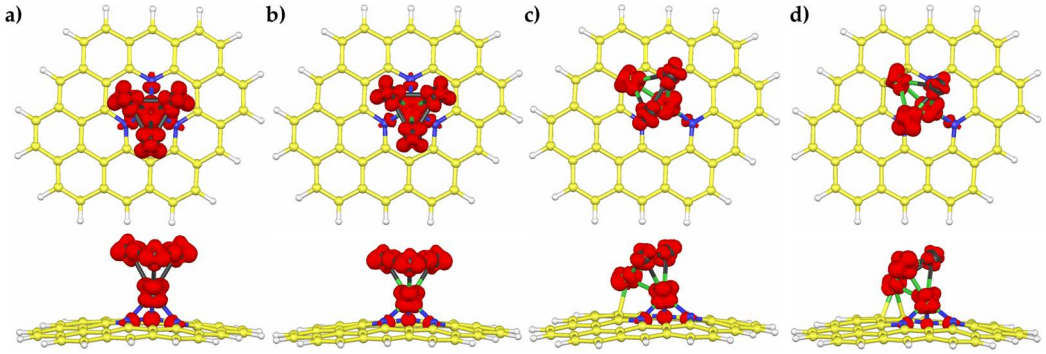

Figure 3. Spin density (red) plots of the $Pd_{4-n}Ni_n$ (n = 0–3) clusters embedded on PNG. (**a**) Pd_4 cluster embedded on PNG, (**b**) Pd_3Ni_1 cluster embedded on PNG, (**c**) Pd_2Ni_2 cluster embedded on PNG, and (**d**) Pd_1Ni_3 cluster embedded on PNG. Blue, yellow, white, green, and black spheres represent N, C, H, Ni, and Pd atoms, respectively.

To complement the discussed interaction between the $Pd_{4-n}Ni_n$ (n = 0–3) clusters and the PNG, BCPs and bond paths were calculated. The computed results are illustrated and reported in Figure 4 and Table 1, respectively. For the Pd_4 cluster embedded on PNG (Figure 4a), three BCPs were located between a Pd atom and three N atoms. For the Pd_3Ni_1 cluster embedded on the PNG (Figure 4b), three BCPs were obtained between a Ni atom and three N atoms. It was observed that between the Pd_2Ni_2 cluster and the PNG (Figure 4c), there were four BCPs, where three were localized between a Ni atom and three N atoms, while the other BCP was localized between a C atom and a Ni atom. Finally, for the Pd_1Ni_3 cluster embedded on the PNG (Figure 4d), five BCPs were computed. Where three BCPs were located between a Ni atom and three N atoms, the other two BCPs were located between a Ni atom and two C atoms.

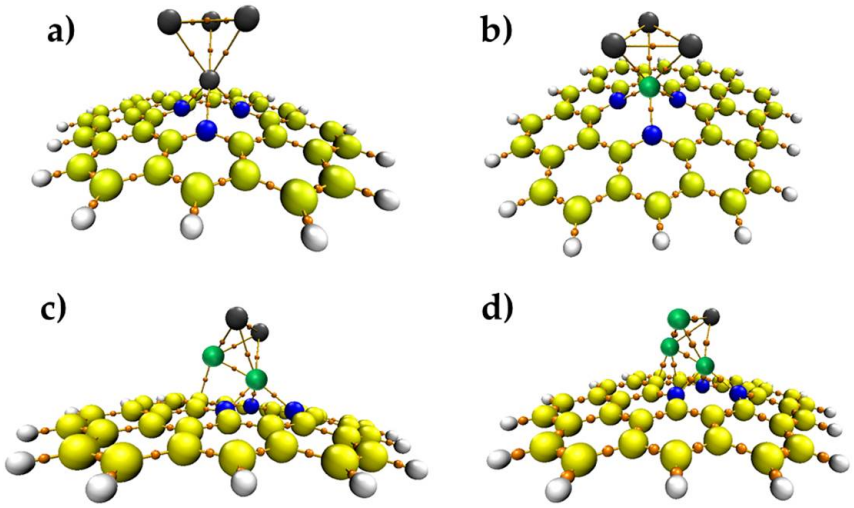

Figure 4. The BCPs (orange spheres) and bond paths between the $Pd_{4-n}Ni_n$ (n = 0–3) clusters and the PNG. (**a**) Pd_4 cluster embedded on PNG, (**b**) Pd_3Ni_1 cluster embedded on PNG, (**c**) Pd_2Ni_2 cluster embedded on PNG, and (**d**) Pd_1Ni_3 cluster embedded on PNG. Blue, yellow, white, green, and black spheres represent N, C, H, Ni, and Pd atoms, respectively.

To better understand the interaction between the $Pd_{4-n}Ni_n$ (n = 0–3) clusters and PNG, the E_{int} and Bader charge transfer were computed (see Table 1). The calculated E_{int} is greater than that calculated in the literature for Pd-based system embedded on pristine graphene [46,47]. Therefore, it was deduced that PNG can be a better support material to stabilize the $Pd_{4-n}Ni_n$ (n = 0–3) clusters. It was observed that as the Ni content increases in the $Pd_{4-n}Ni_n$ (n = 0–3) clusters, the E_{int} between the clusters and PNG tends to increase. Furthermore, the E_{int} calculated for the Pd_4 cluster embedded on PNG is similar to that

calculated in the literature [25,45]. Based on Bader charge analysis, $Pd_{4-n}Ni_n$ (n = 0–3) clusters transfer charge to the PNG because they adopt a positive charge (see Table 1). The calculations revealed that the charge transfer between the clusters and the PNG increases with the number of Ni atoms in the cluster, which can be attributed to the electronegativity of metal atoms, where the electronegativity of the Pd atoms is greater than the Ni atoms. Therefore, Ni atoms can transfer charge more easily. The highest charge transfer from the $Pd_{4-n}Ni_n$ (n = 0–3) clusters to the PNG structure was produced by the metal atoms embedded in the PNG vacancy. It was also observed that C atoms bonded to N atoms transfer charge to the N atoms. When the $Pd_{4-n}Ni_n$ (n = 0–3) clusters are deposited on the PNG structure, N atoms gain the transferred charge (≈−1.07 e per atom), which is attributed to the electronegativity of these atoms. Finally, to investigate the reactivity of the $Pd_{4-n}Ni_n$ (n = 0–3) clusters embedded on PNG, the energy differences between the frontier orbitals (HOMO–LUMO gap) were calculated (see Table 1). The studied composites exhibited a HOMO–LUMO gap less than 1 eV, indicating good reactivity. It was observed that as the Ni content increases in the $Pd_{4-n}Ni_n$ (n = 0–3) clusters, the HOMO–LUMO gap tends to decrease, which can be associated with an improvement in the reactivity of the composites.

3.2. H_2 Adsorption on $Pd_{4-n}Ni_n$ (n = 0–3) Clusters Embedded on PNG

To incorporate novel materials in H_2 storage, it is necessary to calculate the E_{ads} of the H_2 molecule on the materials of interest. In this sense, the H_2 adsorptions on $Pd_{4-n}Ni_n$ (n = 0–3) clusters embedded on PNG were computed. First, the H_2 molecule was optimized, where a H-H bond length of 0.749 Å was calculated, which is very similar to experimental data reported in the literature (0.741 Å) [48]. The most stable H_2 adsorption on $Pd_{4-n}Ni_n$ (n = 0–3) clusters embedded on PNG is illustrated in Figure 5. It was observed that the H_2 molecule was adsorbed on a metal atom of the $Pd_{4-n}Ni_n$ (n = 0–3) clusters embedded on PNG. For the $Pd_{4-n}Ni_n$ (n = 0–2) clusters embedded on PNG, the H_2 adsorption occurs on a Pd atom, whereas for the Pd_1Ni_3 cluster embedded on PNG, the H_2 adsorption occurs on a Ni atom. The calculated interaction mode for the H_2 molecule on Pd_4 embedded on PNG is like that reported in the literature as the most stable adsorption [25]. When the hydrogen molecule is adsorbed on $Pd_{4-n}Ni_n$ (n = 0–3) clusters embedded on PNG, a slight elongation of the H-H bond length is observed (see Table 2), coinciding with previously reported results [25]. On the E_{ads} of the H_2 molecule on $Pd_{4-n}Ni_n$ (n = 0–3) clusters embedded on PNG (see Table 2), the calculated values are less than 0.50 eV, inferring that the H_2 adsorption on $Pd_{4-n}Ni_n$ (n = 0–3) clusters embedded on PNG is via physisorption. Interestingly, the E_{ads} of H_2 molecule comply with the standards specified by the DOE (−0.2 to −0.6 eV/H_2) [15,49]. Consequently, the $Pd_{4-n}Ni_n$ (n = 0–3) clusters embedded on PNG can be viable alternatives for hydrogen storage. Even though the E_{ads} results show that the proposed materials are good candidates for hydrogen storage, future studies should be aimed at evaluating the gravimetric capacity of $Pd_{4-n}Ni_n$ (n = 0–3) clusters embedded on PNG for hydrogen storage.

Table 2. Adsorption energies (E_{int}) and H-H bond length of the H_2 adsorption on $Pd_{4-n}Ni_n$ (n = 0–3) clusters embedded on PNG.

	Pd_4/PNG	**Pd_3Ni_1/PNG**	**Pd_2Ni_2/PNG**	**Pd_1Ni_3/PNG**
E_{ads} (eV)	−0.29	−0.31	−0.39	−0.37
H-H bond lengths (Å)	0.83	0.83	0.84	0.85

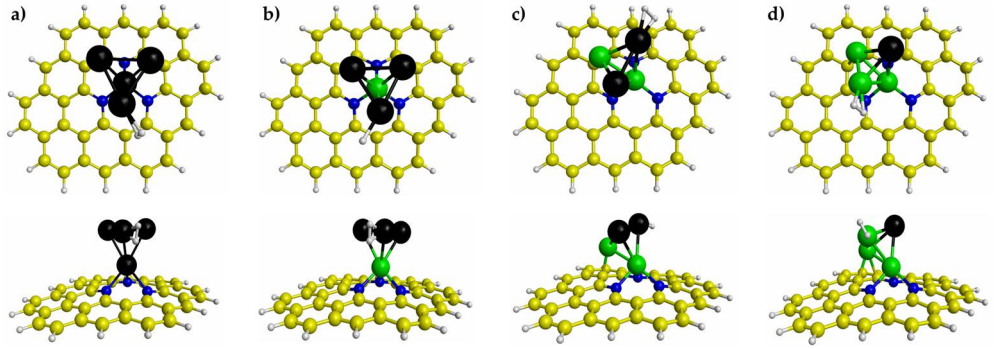

Figure 5. The most stable H_2 adsorptions on $Pd_{4-n}Ni_n$ (n = 0–3) clusters embedded on PNG. (**a**) H_2 adsorption on Pd_4 cluster embedded on PNG, (**b**) H_2 adsorption on Pd_3Ni_1 cluster embedded on PNG, (**c**) H_2 adsorption on Pd_2Ni_2 cluster embedded on PNG, and (**d**) H_2 adsorption on Pd_1Ni_3 cluster embedded on PNG. Blue, yellow, white, green, and black spheres represent N, C, H, Ni, and Pd atoms, respectively.

4. Conclusions

In this study, the H_2 adsorption on $Pd_{4-n}Ni_n$ (n = 0–3) clusters embedded on PNG was studied, employing DFT computations. To the best of the authors' knowledge, this is the first DFT-based study on the H_2 adsorption on these composites. Based on the E_{int} between the $Pd_{4-n}Ni_n$ (n = 0–3) clusters and the PNG, it was observed that the E_{int} was greater than that calculated in the literature for Pd-based clusters embedded on pristine graphene. Therefore, it has been deduced that PNG can be a good support material to stabilize the $Pd_{4-n}Ni_n$ (n = 0–3) clusters. Further, the analyzed composites exhibit a HOMO–LUMO gap less than 1 eV, indicating good reactivity. According to the E_{ads} of H_2 on the $Pd_{4-n}Ni_n$ (n = 0–3) clusters embedded on PNG, it was observed that the systems studied meet the standards specified by the DOE. Consequently, these composites can be viable alternatives for hydrogen storage.

Author Contributions: Conceptualization, B.G.-H., L.S.-S. and A.V.-G.; methodology, B.G.-H., L.S.-S. and A.V.-G.; formal analysis, B.G.-H. and A.G.-S.; investigation, B.G.-H., L.S.-S. and A.V.-G.; writing—original draft preparation, A.G.-S., V.A.F.-L. and H.C.-M.; writing—review and editing, V.A.F.-L. and H.C.-M.; funding acquisition, B.G.-H. and H.C.-M. All authors have read and agreed to the published version of the manuscript.

Funding: This research was funded by Tecnológico Nacional de México, grant number 19057.23-P.

Data Availability Statement: Data are contained within the article.

Conflicts of Interest: The authors declare no conflicts of interest.

References

1. Abdin, Z.; Zafaranloo, A.; Rafiee, A.; Mérida, W.; Lipiński, W.; Khalilpour, K.R. Hydrogen as an energy vector. *Renew. Sust. Energ. Rev.* **2020**, *120*, 109620. [CrossRef]
2. Nazir, H.; Louis, C.; Jose, S.; Prakash, J.; Muthuswamy, N.; Buan, M.E.; Kannan, A.M. Is the H_2 economy realizable in the foreseeable future? Part I: H_2 production methods. *Int. J. Hydrogen Energy* **2020**, *45*, 13777–13788. [CrossRef]
3. Jain, I.P. Hydrogen the fuel for 21st century. *Int. J. Hydrogen Energy* **2009**, *34*, 7368–7378. [CrossRef]
4. Moradi, R.; Groth, K.M. Hydrogen storage and delivery: Review of the state of the art technologies and risk and reliability analysis. *Int. J. Hydrogen Energy* **2019**, *44*, 12254–12269. [CrossRef]
5. Durbin, D.J.; Malardier-Jugroot, C. Review of hydrogen storage techniques for on board vehicle applications. *Int. J. Hydrogen Energy* **2013**, *38*, 14595–14617. [CrossRef]
6. Niaz, S.; Manzoor, T.; Pandith, A.H. Hydrogen storage: Materials, methods and perspectives. *Renew. Sust. Energ. Rev.* **2015**, *50*, 457–469. [CrossRef]
7. Ren, J.; Musyoka, N.M.; Langmi, H.W.; Mathe, M.; Liao, S. Current research trends and perspectives on materials-based hydrogen storage solutions: A critical review. *Int. J. Hydrogen Energy* **2017**, *42*, 289–311. [CrossRef]
8. Yang, J.; Sudik, A.; Wolverton, C.; Siegel, D.J. High capacity hydrogen storage materials: Attributes for automotive applications and techniques for materials discovery. *Chem. Soc. Rev.* **2010**, *39*, 656–675. [CrossRef] [PubMed]

9. Kumar, P.; Singh, S.; Hashmi, S.A.R.; Kim, K.H. MXenes: Emerging 2D materials for hydrogen storage. *Nano Energy* **2021**, *85*, 105989. [CrossRef]
10. Gupta, A.; Baron, G.V.; Perreault, P.; Lenaerts, S.; Ciocarlan, R.G.; Cool, P.; Denayer, J.F. Hydrogen clathrates: Next generation hydrogen storage materials. *Energy Storage Mater.* **2021**, *41*, 69–107. [CrossRef]
11. Jena, P. Materials for hydrogen storage: Past, present, and future. *J. Phys. Chem. Lett.* **2011**, *2*, 206–211. [CrossRef]
12. Yartys, V.A.; Lototskyy, M.V.; Akiba, E.; Albert, R.; Antonov, V.E.; Ares, J.R.; Zhu, M. Magnesium based materials for hydrogen based energy storage: Past, present and future. *Int. J. Hydrogen Energy* **2019**, *44*, 7809–7859. [CrossRef]
13. Mohan, M.; Sharma, V.K.; Kumar, E.A.; Gayathri, V. Hydrogen storage in carbon materials—A review. *Energy Storage* **2019**, *1*, e35. [CrossRef]
14. Tozzini, V.; Pellegrini, V. Prospects for hydrogen storage in graphene. *Phys. Chem. Chem. Phys.* **2013**, *15*, 80–89. [CrossRef]
15. Cruz-Martínez, H.; García-Hilerio, B.; Montejo-Alvaro, F.; Gazga-Villalobos, A.; Rojas-Chávez, H.; Sánchez-Rodríguez, E.P. Density functional theory-based approaches to improving hydrogen storage in graphene-based materials. *Molecules* **2024**, *29*, 436. [CrossRef]
16. Jukk, K.; Kongi, N.; Rauwel, P.; Matisen, L.; Tammeveski, K. Platinum nanoparticles supported on nitrogen-doped graphene nanosheets as electrocatalysts for oxygen reduction reaction. *Electrocatalysis* **2016**, *7*, 428–440. [CrossRef]
17. Gracia-Espino, E.; Jia, X.; Wågberg, T. Improved oxygen reduction performance of Pt–Ni nanoparticles by adhesion on nitrogen-doped graphene. *J. Phys. Chem. C* **2014**, *118*, 2804–2811. [CrossRef]
18. Ortiz-Vázquez, E.A.; Montejo-Alvaro, F.; Cruz-Martínez, H.; Calaminici, P. Theoretical study of PdNi and PdCu clusters embedded on graphene modified by monovacancy and nitrogen doping. *J. Comput. Chem.* **2024**, *45*, 1744–1749. [CrossRef] [PubMed]
19. Sánchez-Rodríguez, E.P.; Vargas-Hernández, C.N.; Cruz-Martínez, H.; Medina, D.I. Stability, magnetic, energetic, and reactivity properties of icosahedral M@Pd_{12} (M = Fe, Co, Ni, and Cu) core-shell nanoparticles supported on pyridinic N_3-doped graphene. *Solid State Sci.* **2021**, *112*, 106483. [CrossRef]
20. Jalili, S.; Goliaei, E.M.; Schofield, J. Silver cluster supported on nitrogen-doped graphene as an electrocatalyst with high activity and stability for oxygen reduction reaction. *Int. J. Hydrogen Energy* **2017**, *42*, 14522–14533. [CrossRef]
21. Martínez-Espinosa, J.A.; Cruz-Martínez, H.; Calaminici, P.; Medina, D.I. Structures and properties of $Co_{13-x}Cu_x$ (x = 0–13) nanoclusters and their interaction with pyridinic N_3-doped graphene nanoflake. *Phys. E* **2021**, *134*, 114858. [CrossRef]
22. Wang, Q.; Tian, Y.; Chen, G.; Zhao, J. Theoretical insights into the energetics and electronic properties of MPt_{12} (M = Fe, Co, Ni, Cu, and Pd) nanoparticles supported by N-doped defective graphene. *Appl. Surf. Sci.* **2017**, *397*, 199–205. [CrossRef]
23. Cruz-Martínez, H.; Rojas-Chávez, H.; Valdés-Madrigal, M.A.; López-Sosa, L.; Calaminici, P. Stability and catalytic properties of Pt–Ni clusters supported on pyridinic N-doped graphene nanoflakes: An auxiliary density functional theory study. *Theor. Chem. Acc.* **2022**, *141*, 46. [CrossRef]
24. Montejo-Alvaro, F.; Martínez-Espinosa, J.A.; Rojas-Chávez, H.; Navarro-Ibarra, D.C.; Cruz-Martínez, H.; Medina, D.I. CO_2 Adsorption over 3d Transition-Metal Nanoclusters Supported on Pyridinic N_3-Doped Graphene: A DFT Investigation. *Materials* **2022**, *15*, 6136. [CrossRef] [PubMed]
25. Rangel, E.; Sansores, E. heoretical study of hydrogen adsorption on nitrogen doped graphene decorated with palladium clusters. *Int. J. Hydrogen Energy* **2014**, *39*, 6558–6566. [CrossRef]
26. Rangel, E.; Sansores, E.; Vallejo, E.; Hernández-Hernández, A.; López-Pérez, P.A. Study of the interplay between N-graphene defects and small Pd clusters for enhanced hydrogen storage via a spill-over mechanism. *Phys. Chem. Chem. Phys.* **2016**, *18*, 33158–33170. [CrossRef] [PubMed]
27. Luo, Z.; Fan, X.; Pan, R.; An, Y. A first-principles study of Sc-decorated graphene with pyridinic-N defects for hydrogen storage. *Int. J. Hydrogen Energy* **2017**, *42*, 3106–3113. [CrossRef]
28. Ambrusi, R.E.; Pronsato, M.E. DFT study of Rh and Ti dimers decorating N-doped pyridinic and pyrrolic graphene for molecular and dissociative hydrogen adsorption. *Appl. Surf. Sci.* **2019**, *464*, 243–254. [CrossRef]
29. Singla, M.; Jaggi, N. Enhanced hydrogen sensing properties in copper decorated nitrogen doped defective graphene nanoribbons: DFT study. *Phys. E* **2021**, *131*, 114756. [CrossRef]
30. Cruz-Martínez, H.; Guerra-Cabrera, W.; Flores-Rojas, E.; Ruiz-Villalobos, D.; Rojas-Chávez, H.; Peña-Castañeda, Y.A.; Medina, D.I. Pt-free metal nanocatalysts for the oxygen reduction reaction combining experiment and theory: An overview. *Molecules* **2021**, *26*, 6689. [CrossRef]
31. Sanij, F.D.; Balakrishnan, P.; Leung, P.; Shah, A.; Su, H.; Xu, Q. Advanced Pd-based nanomaterials for electro-catalytic oxygen reduction in fuel cells: A review. *Int. J. Hydrogen Energy* **2021**, *46*, 14596–14627. [CrossRef]
32. Geudtner, G.; Calaminici, P.; Carmona-Espíndola, J.; del Campo, J.M.; Domínguez-Soria, V.D.; Moreno, R.F.; Gamboa, G.U.; Goursot, A.; Köster, A.M.; Salahub, D.R.; et al. DeMon2k. *WIREs Comput. Mol. Sci.* **2012**, *2*, 548–555. [CrossRef]
33. Zhang, Y.; Yang, W. Comment on "Generalized gradient approximation made simple". *Phys. Rev. Lett.* **1998**, *80*, 890. [CrossRef]
34. Mintmire, J.W.; Dunlap, B.I. Fitting the Coulomb potential variationally in linear-combination-of-atomic-orbitals density-functional calculations. *Phys. Rev. A* **1982**, *25*, 88. [CrossRef]
35. Andrae, D.; Haeussermann, U.; Dolg, M.; Stoll, H.; Preuss, H. Energy-adjusted ab initio pseudopotentials for the second and third row transition elements. *Theor. Chim. Acta* **1990**, *77*, 123–141. [CrossRef]
36. Calaminici, P.; Janetzko, F.; Köster, A.M.; Mejia-Olvera, R.; Zuniga-Gutierrez, B. Density functional theory optimized basis sets for gradient corrected functionals: 3d transition metal systems. *J. Chem. Phys.* **2007**, *126*, 044108. [CrossRef] [PubMed]

37. Köster, A.M.; Reveles, J.U.; del Campo, J.M. Calculation of exchange-correlation potentials with auxiliary function densities. *J. Chem. Phys.* **2004**, *121*, 3417–3424. [CrossRef] [PubMed]
38. Reveles, J.U.; Köster, A.M. Geometry optimization in density functional methods. *J. Comput. Chem.* **2004**, *25*, 1109–1116. [CrossRef]
39. Cervantes-Flores, A.; Cruz-Martínez, H.; Solorza-Feria, O.; Calaminici, P. A first-principles study of Ni_nPd_n (n = 1–5) clusters. *J. Mol. Model.* **2017**, *23*, 161. [CrossRef]
40. Cruz-Martínez, H.; López-Sosa, L.; Solorza-Feria, O.; Calaminici, P. First-principles investigation of adsorption and dissociation of molecular oxygen on pure Pd, Ni-doped Pd and NiPd alloy clusters. *Int. J. Hydrogen Energy* **2017**, *42*, 30310–30317. [CrossRef]
41. Roy, G.; Chattopadhyay, A.P. The reactivity of CO on bimetallic Ni_3M clusters (M = Sc, Ti, V, Cr, Mn, Fe, Co, Cu, Rh, Ru, Ag, Pd and Pt) by density functional theory. *New J. Chem.* **2019**, *43*, 11363–11373. [CrossRef]
42. Domancich, N.F.; Ferullo, R.M.; Castellani, N.J. Interaction of aluminum dimer with defective graphene. *Comput. Theor. Chem.* **2015**, *1059*, 27–34. [CrossRef]
43. Nieman, R.; Aquino, A.J.; Hardcastle, T.P.; Kotakoski, J.; Susi, T.; Lischka, H. Structure and electronic states of a graphene double vacancy with an embedded Si dopant. *J. Chem. Phys.* **2017**, *147*, 194702. [CrossRef] [PubMed]
44. Ferro, Y.; Teillet-Billy, D.; Rougeau, N.; Sidis, V.; Morisset, S.; Allouche, A. Stability and magnetism of hydrogen dimers on graphene. *Phys. Rev. B* **2008**, *78*, 085417. [CrossRef]
45. Zhao, C.; Wu, H. Density functional investigation of mercury and arsenic adsorption on nitrogen doped graphene decorated with palladium clusters: A promising heavy metal sensing material in farmland. *Appl. Surf. Sci.* **2017**, *399*, 55–66. [CrossRef]
46. Montejo-Alvaro, F.; Rojas-Chávez, H.; Román-Doval, R.; Mtz-Enriquez, A.I.; Cruz-Martínez, H.; Medina, D.I. Stability of Pd clusters supported on pristine, B-doped, and defective graphene quantum dots, and their reactivity toward oxygen adsorption: A DFT analysis. *Solid State. Sci.* **2019**, *93*, 55–61. [CrossRef]
47. Rêgo, C.R.; Tereshchuk, P.; Oliveira, L.N.; Da Silva, J.L. Graphene-supported small transition-metal clusters: A density functional theory investigation within van der Waals corrections. *Phys. Rev. B* **2017**, *95*, 235422. [CrossRef]
48. Huber, K.P.; Herzberg, G. *Molecular Spectra and Molecular Structure: IV. Constants of Diatomic Molecules*; Van Nostrand Reinhold Inc.: New York, NY, USA, 1979.
49. Jin, X.; Qi, P.; Yang, H.; Zhang, Y.; Li, J.; Chen, H. Enhanced hydrogen adsorption on Li-coated $B_{12}C_6N_6$. *J. Chem. Phys.* **2016**, *145*, 164301. [CrossRef]